

# Hierarchically Designed CNF/S–Cu/CNF Nonwoven Electrode as Free-Standing Cathode for Lithium–Sulfur Batteries

Zihao Bian<sup>+</sup><sup>[a]</sup>, Ying Xu<sup>+</sup><sup>[a]</sup>, Tao Yuan<sup>[a]</sup>, Chengxin Peng<sup>[a]</sup>, Yuepeng Pang<sup>[a]</sup>, Junhe Yang<sup>[a]</sup> and Shiyou Zheng\*<sup>[a]</sup>

A flexible lithium–sulfur (Li–S) battery cathode is prepared through uniformly depositing sulfur solution into an electrospun N-rich and Cu-decorated nonwoven carbon nanofiber (CNF) film to form sandwich structured CNF/S–Cu/CNF film electrodes. As a free-standing cathode of Li–S battery, the unique structural CNF/S–Cu/CNF composite cathodes exhibit high capacity and rate capability as well as long cycling stability. The electrodes can deliver a reversible capacity of 1295 mAh g<sup>-1</sup> at a current density of 0.1 A g<sup>-1</sup>, and maintain more than

530 mAh g<sup>-1</sup> even at a high current rate of 1 A g<sup>-1</sup> after 300 cycles along with a Coulombic efficiency close to 100%. The exceptional performance of CNF/S–Cu/CNF as cathode in Li–S batteries is attributed to a synergistic contribution from the CNF layers, the decorated-Cu nanoparticles and the doped N element in CNF, which can physically and chemically stabilize S and provide fast electronic conductivity. This facile strategy will pave the way to construct high-performance flexible Li–S batteries.

## 1. Introduction

Owning to the ultrahigh theoretical capacity (1675 mAh g<sup>-1</sup>), energy density (2600 Wh kg<sup>-1</sup>) and abundant resources, the Li–S battery has been considered as the most promising alternatives for next generation electrochemical energy storage systems.<sup>[1–2]</sup> However, the Li–S battery is still not commercialized at present, most probably attributed to many issues in the sulfur cathode, including: i) insulating nature of S leading to poor battery kinetic; ii) low S loading and utilization resulting in low overall capacity; iii) dissolution of lithium polysulfide and the “shuttle reaction” causing poor cycle life.<sup>[3–5]</sup>

In order to solve or alleviate these problems, many strategies have been proposed. In all the improvement approaches, construction of electric conductive frameworks, such as carbon nanotubes (CNTs),<sup>[6]</sup> graphene,<sup>[7]</sup> carbon fibers,<sup>[8]</sup> conductive polymers<sup>[9]</sup> and their hybrids,<sup>[10]</sup> has been considered as the most successful technique for improving the electrochemical correspondence for sulfur cathode. However, conventional carbon materials always limited the sulfur loading (less than 40%) in the entire cathode structure.<sup>[11]</sup> Moreover, the unmodified carbon materials usually fail to restrict the dissolution and shuttling of polysulfide.<sup>[12]</sup>

Introducing transition metals or nonmetallic heteroatoms is an effective strategy for chemical sulfur fixation.<sup>[13,14]</sup> Some research groups studied the adsorption behavior between

polysulfides and transition metal or metal oxides by First-Principles based on the bond energy, space structure and charge transfer.<sup>[15]</sup> It is found that sulfidation can cause strong interactions between metal atoms and polysulfides, which is the key factor in improving battery performance.<sup>[16]</sup> Among all transition metals, Cu is a promising candidate due to it is highly conductive and easy to form CuS<sub>x</sub> just only coating S onto Cu foil at 60 °C.<sup>[17,18]</sup> Additionally, doping nonmetallic heteroatoms (e.g. B, N, O, et al) into cathodic materials of Li–S battery has also been proved to be an effective way for inhibiting the polysulfide shuttle.<sup>[19]</sup> Song et al. carried out a theoretical study of the nitrogen-doped carbon/sulfur cathode to demonstrate the nitrogen doping can efficiently limit the dissolution of lithium polysulfide, by promoting the chemical reaction between lithium polysulfide (Li<sub>2</sub>S<sub>4</sub>, Li<sub>2</sub>S<sub>6</sub>, Li<sub>2</sub>S<sub>8</sub>) and defects sites in carbon.<sup>[20]</sup>

With development of high energy density Li–S battery systems and more lightweight and bendable batteries for potential application in flexible electronic devices, the flexible and free-standing electrode using less non-active material are significant.<sup>[21]</sup> Herein we propose a facile strategy to construct flexible sandwich structural nonwoven CNF/S–Cu/CNF cathodes for Li–S batteries by uniformly depositing sulfur into N-rich and Cu-decorated nonwoven. As a free-standing cathode of Li–S battery, the unique structural CNF/S–Cu/CNF composite cathode presents high capacity, super rate capability and long cycle stability. It has been found that the copper nanoparticles embedded in the inner CNF layers and the nitrogen elements doped in the whole CNF films can effectively prevent shuttle effect of polysulfides, meanwhile, the cross-linked long CNF provide flexible and robust supporter, which are helpful to improve sulfur utilization and promote the rate and cycle abilities of CNF/S–Cu/CNF cathode.<sup>[22,23]</sup> The results demonstrated will provide a new material design strategy to achieve

[a] Z. Bian,<sup>†</sup> Y. Xu,<sup>†</sup> T. Yuan, C. Peng, Y. Pang, Prof. J. Yang, S. Zheng  
School of Materials Science and Engineering  
University of Shanghai for Science and Technology  
Shanghai, 200093, China  
E-mail: syzheng@usst.edu.cn

[†] These authors contributed equally to this work.

 Supporting information for this article is available on the WWW under <https://doi.org/10.1002/batt.201900014>

high overall performance of sulfur cathodes for flexible Li–S batteries.

## 2. Results and Discussion

### 2.1. Structural and Morphological Features

The typical procedure, morphologies and structural mechanism for the synthesis sandwich structural CNF/S–Cu/CNF cathode are shown schematically in Figure 1. The PAN layer is firstly prepared by electrospinning technology. And another layer of PAN/Cu(NO<sub>3</sub>)<sub>2</sub> is continued to electrospun on the PAN layer to form a PAN–PAN/Cu(NO<sub>3</sub>)<sub>2</sub> double layer film.

After pre-oxidizing at 280 °C in the air atmosphere and further carbonizing at 800 °C in N<sub>2</sub> atmosphere, the CNF–CNF/Cu double layer film is prepared. Then the sulfur, with a same weigh of CNF–CNF/Cu film, is coated on the CNF/Cu side. Two pieces of sulfur impregnated sheets are stacked together, with

sulfur face to face way. After further heating at 150 °C in a sealed box, the sulfur, with a state of liquid/gaseous, has been dispersed uniformly in the CNF/S–Cu/CNF composite. The fibers in the obtained CNF/S–Cu/CNF sample exhibit smooth surface and no obvious Cu nanoparticles on the surface, which is very similar as the material reported in our previous work.<sup>[24]</sup> In our previous work, a CNF/Cu composites prepared by the same process presented smooth, regular, and long fibrous morphologies with Cu nanoparticles percolating throughout the carbon matrix.<sup>[24]</sup> Meanwhile, the copper nanoparticles and sulfur atoms in the middle of CNF/S–Cu/CNF films had a chemical reaction to became CuS<sub>x</sub>, which will be proved in the following X-ray photoelectron spectroscopy (XPS) analysis.

The as-obtained CNF/S–Cu/CNF film is exhibited great flexibility and sandwich structure, as shown in Figure 2a and b, respectively. The cross-linked CNF provide a framework with good electric conductive for sulfur. And the corresponding energy dispersive X-ray spectrometry (EDS) mappings of elemental distribution in the Figure 2b and S1a further prove

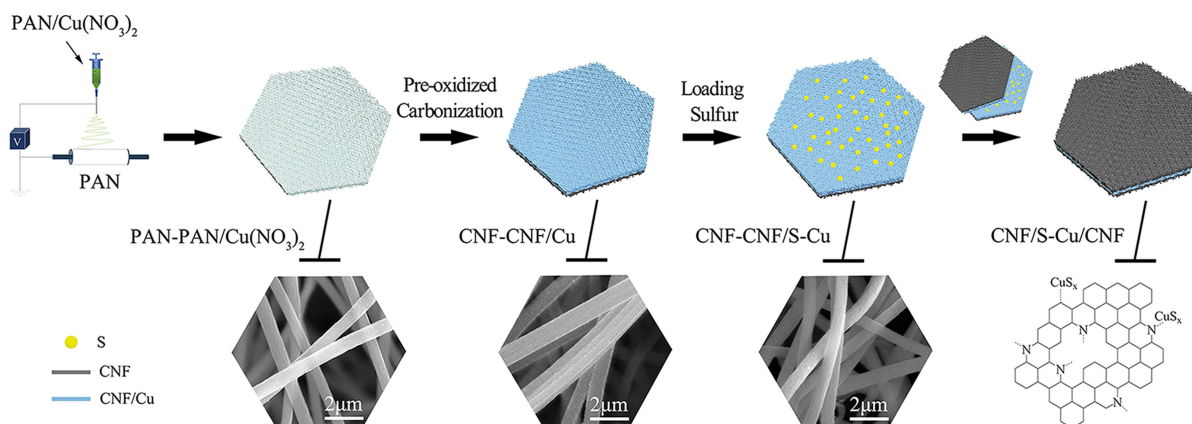


**Figure 1.** Schematic illustration and corresponding SEM images of preparation for CNF/S–Cu/CNF composites.

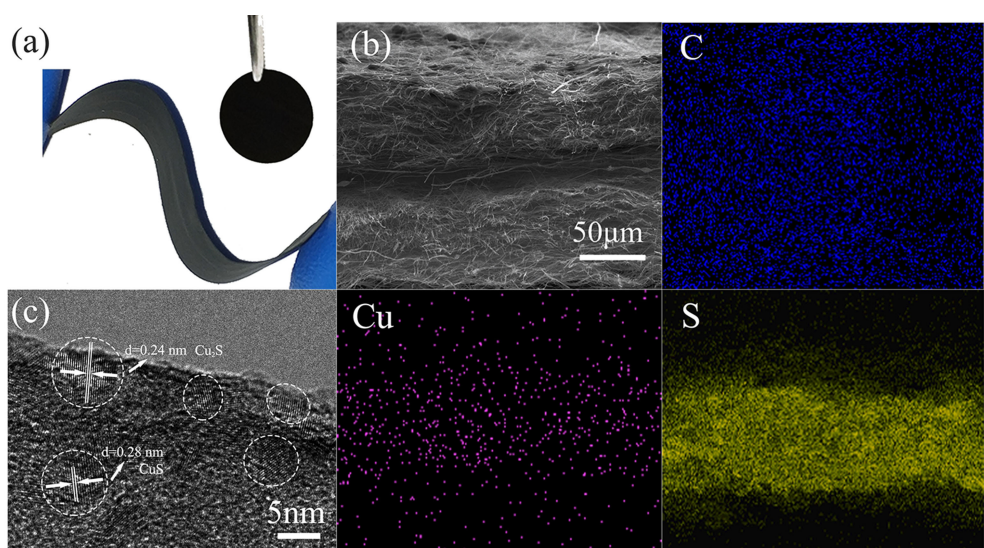


**Figure 2.** a) The digital photos of flexible CNF/S–Cu/CNF electrode and b) SEM image of the CNF/S–Cu/CNF cathode with the corresponding elemental mappings of carbon, copper and sulfur; c) TEM image of the CNF/S–Cu/CNF material.

that the sulfur and copper concentrated in the middle of CNF/S–Cu/CNF film, and large amount of nitrogen atoms (about 5.4 at% obtained by element analysis) distributed throughout the CNF/S–Cu/CNF film. The high-resolution TEM (HR-TEM) image of CNF/S–Cu/CNF composite in Figure 2c clearly shows that the CuS<sub>x</sub> nanoparticles are well dispersed in the CNF/S–Cu/CNF composites. The lattice spacing of 0.28 and 0.24 nm corresponds to (103) plane of cubic CuS (PDF04-0464) and (204) plane of Cu<sub>2</sub>S (PDF33-0490), indicating the formation of CuS<sub>x</sub> within the fiber matrix after heating. This kind of structure is expected to restrict the shuttle effect of polysulfides.<sup>[25]</sup> The contents of each element calculated by EDS are shown in Figure S1b. Owing to the loss of sulfur during the final heat process, the real sulfur content in the CNF/S–Cu/CNF film is ~45 wt.% according to the TGA result (Figure S2). From the TGA curves, the evaporation of pure S and S in the CNF/S/CNF begin at ~200 °C and end at ~300 °C. However, the TGA curve of CNF/S–Cu/CNF sample is different from them, which exhibits another delayed weight loss (about 15%) above 300 °C. The delay in releasing S from CNF/S–Cu/CNF sample confirms that S is indeed stabilized by Cu nanoparticles in the CNF/S–Cu/CNF film, which is attributed to the strong interaction between Cu and S. According to the XRD patterns in Figure S3, the crystal structure of sulfur in CNF/S–Cu/CNF film is a typical S<sub>8</sub> molecular structure.<sup>[26,27]</sup> And the as-prepared CNF tend to be

an amorphous structure according to the Raman result (Figure S4).<sup>[28]</sup>

More information about the chemical interaction of the elements in CNF/S–Cu/CNF film is characterized by XPS analysis. As shown in Figure 3a, the CNF/S–Cu/CNF film mainly included C, O, S, N and a small amount of Cu, originating from the PAN molecules (C, O and N), and the added S and Cu. The contents of Cu and S obtained from XPS results are much lower than added. This is because most of the Cu and S in the middle of the film cannot be captured by XPS. The XPS characterization technology only reflects the surface element information within the depth of 3 nm.<sup>[29]</sup> The S 2p and Cu 2p high-resolution XPS analyses shown in Figure 3b, c further prove the interaction between S and Cu. As shown in Figure 3b, The S 2p spectrum can be decomposed into four peaks. Two peaks located at around 163.0 and 164.1 eV are attributed to spin orbit coupling of S 2p<sup>1/2</sup> and S 2p<sup>3/2</sup>, respectively. The lower binding energy due to the existence of the bridging sulfur and terminal sulfur.<sup>[30,31]</sup> In addition, the peaks located at 167.1 and 168.6 eV are assigned to the appearance of Cu-polysulfides and sulfate, which proves the interaction between sulfur and copper.<sup>[32]</sup> Further evidence is supported by the Cu 2p XPS spectra. As shown in Figure 3c, the Cu 2p spectrum can be fitted by four peaks (931.3, 933.4, 951.3 and 953.3 eV), which are assigned to Cu<sup>+</sup> 2p<sup>3/2</sup>, Cu<sup>2+</sup> 2p<sup>3/2</sup>, Cu<sup>+</sup> 2p<sup>1/2</sup> and Cu<sup>2+</sup> 2p<sup>1/2</sup>, respectively.<sup>[13]</sup> It indicates that the chemical valences of Cu in the CNF/S–Cu/

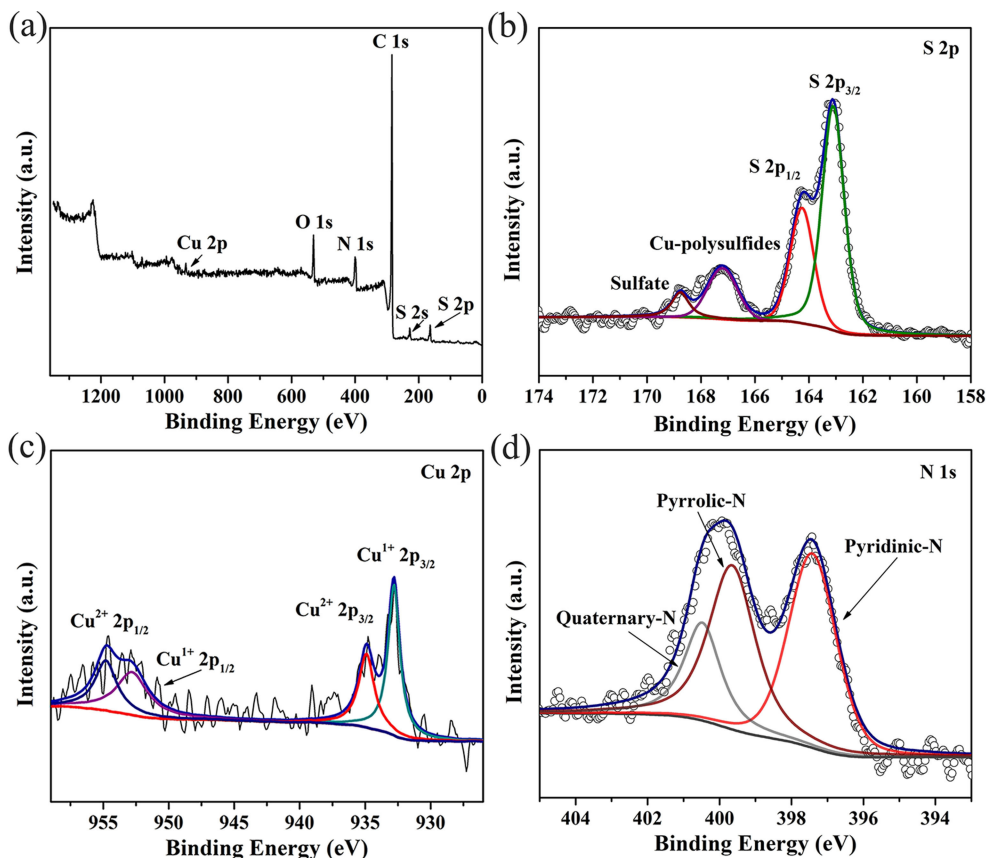


**Figure 3.** X-ray photoelectron spectra of the CNF/S–Cu/CNF electrode (a) and corresponding S 2p (b), Cu 2p (c) and N 1s (d) high-resolution XPS analyses.

CNF film are in mixture valence states of +1 and +2, implying the formation of CuS<sub>x</sub>. Furthermore, it is also worth noting that the high N-doping will help to prevent the shuttle reaction of polysulfide.<sup>[33]</sup> As shown in Figure 3d, The N 1s peaks in the XPS spectra of CNF/S–Cu/CNF sample are fitted into three peaks, which are pyridinic-N (at 397.4 eV), pyrrolic-N (at 399.6 eV) and quaternary-N (at 400.2 eV), respectively.<sup>[27,34–36]</sup> A high ratio of pyridinic-N (41.3% at.%) (i.e. N that located at the edge by replacing a carbon atom on the six-membered ring in the graphite) indicates that better lithium polysulfide chemisorption activity will be reflected in the CNF/S–Cu/CNF film electrode.<sup>[37]</sup>

## 2.2. Electrode Performance

For comparison, a symmetrical CNF/S/CNF sandwich structural film without Cu nanoparticles is synthesized in the same way. Figure 4a shows the initial cyclic voltammetric (CV) curves of the CNF/S–Cu/CNF electrode in the potential range of 1.5–3.0 V. Two distinct cathodic peaks appear at 2.4 and 2.0 V associate with the transition from S<sub>8</sub> to soluble higher order polysulfides (Li<sub>2</sub>S<sub>x</sub>, 4 ≤ x ≤ 8).<sup>[38–40]</sup> Another broad peak occur at a lower potential about 1.8 V is attributed to the transition from soluble higher polysulfides to insoluble lower polysulfides (Li<sub>2</sub>S<sub>2</sub> or Li<sub>2</sub>S) and the initial decomposition of LiNO<sub>3</sub>.<sup>[41]</sup> In the subsequent anodic process, oxidation peaks are observed at 2.1, 2.4 and

2.6 V, which are attributed to the reverse phase transition from Li<sub>2</sub>S to polysulfides and finally to sulfur.<sup>[42]</sup> After the first cycle, the cathode peak shifts toward low potential slightly accompanying with the electrochemical activation of CNF/S–Cu/CNF cathode.<sup>[43]</sup> Other than the first cycle, the CV curves overlap very well from the second to the fifth cycles, indicating good reversibility of lithiation and delithiation process of CNF/S–Cu/CNF film electrode. As shown in Figure 4b, the CNF/S/CNF sample also exhibit similar CV curves as before, which also exhibit the redox reaction of S cathode. However, the delivery current is lower, implying that the CNF/S/CNF sample without Cu has an inferior electrochemical reversibility.

The voltage profiles for the initial five discharge/charge cycles of the CNF/S–Cu/CNF film electrode at a current density of 100 mA g<sup>-1</sup> are presented in Figure 4c. From the discharge curves, three voltage plateaus at ~2.3, 2.1 and 1.8 V can be observed, which correspond to the lithiation process of S<sub>8</sub> to form soluble higher order polysulfides (Li<sub>2</sub>S<sub>x</sub>, 4 ≤ x ≤ 8) finally to insoluble low-order polysulfides Li<sub>2</sub>S<sub>2</sub> and/or Li<sub>2</sub>S and in agreement with the peaks in the CV.<sup>[44,45]</sup> The first lithiation capacity of the CNF/S–Cu/CNF film electrode is 1612 mAh g<sup>-1</sup>, which is closed to the theoretical capacity of S (1675 mAh g<sup>-1</sup>). And the reversible discharge capacity is 1295 mAh g<sup>-1</sup> with a high initial Coulombic efficiency of 91.7%. The CNF/S/CNF electrode in comparison in Figure 4d, however, shows the similar initial discharge capacity but much lower reversible capacity of

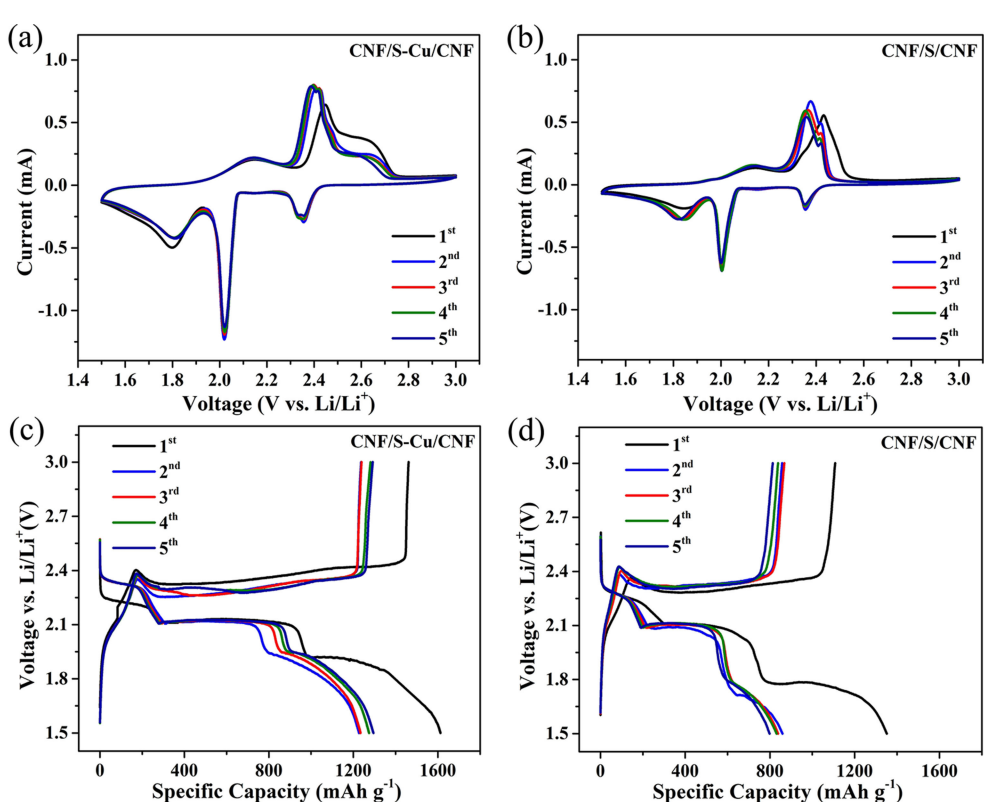


**Figure 4.** Electrochemical properties of the CNF/S–Cu/CNF and CNF/S/CNF electrodes. CV curves of CNF/S–Cu/CNF (a) and CNF/S/CNF (b) electrode between 1.5 and 3.0 V in Li–S batteries at 0.2 mV s<sup>-1</sup>; charge/discharge voltage profiles of CNF/S–Cu/CNF (c) and CNF/S/CNF (d) electrode in the initial five cycles at a current density of 0.1 A g<sup>-1</sup>.

798  $\text{mAh g}^{-1}$ , which most probably because of the lack of Cu nanoparticles as the anchor holding sulfur in the electrode.

The differences of electrochemical response between CNF/S–Cu/CNF and CNF/S/CNF electrodes can be more clearly reflected by rate performance testing. As shown in Figure 5a, reversible capacities of 1085, 953, 830, 742, 647, 540, 455 and 430  $\text{mAh g}^{-1}$  are obtained at 0.1, 0.2, 0.5, 1, 2, 4, 6 and 8  $\text{A g}^{-1}$  respectively for CNF/S–Cu/CNF electrode. When the charge/discharge rate changes back to 0.2  $\text{A g}^{-1}$  after 130 cycles, a high reserved capacity of 727  $\text{mAh g}^{-1}$  is obtained from CNF/S–Cu/CNF electrode, showing a great merit for tolerance of harsh current densities. By comparison, the capacity degradation of the CNF/S/CNF electrode is significantly obvious with the CNF/S–Cu/CNF electrode upon increasing current density. When the current density up to 0.5  $\text{A g}^{-1}$ , the CNF/S/CNF electrode shows a sharp drop in capacity. The superior rate performance of CNF/S–Cu/CNF electrode is attributed to the small polarization, which can be reflected in plateau potentials margin at various current rates from Figure 5b.<sup>[46,47]</sup> The charge/discharge curves exhibit very flat potential platforms even at a very high current density of 8  $\text{A g}^{-1}$ , indicating a fast electrochemical response for the CNF/S–Cu/CNF electrode. Furthermore, Figure 5c depicts the electrochemical impedance spectroscopy (EIS) of the Li–S battery based on two film electrode. The parameters extracted from the related equivalent circuit are listed in Table S1. As shown in Table S1, CNF/S–Cu/CNF film electrode exhibits a charge transfer resistance ( $R_{ct}$ ) of 69.6  $\Omega$ , much smaller than that of the CNF/S/CNF electrode (112.6  $\Omega$ ), which indicate that Cu-containing fiber electrode is benefit to enhance the electrochemical kinetics and reduce the interphase resistance.<sup>[48,49]</sup>

The cycle performance of CNF/S–Cu/CNF and CNF/S/CNF film electrodes under a high current rate of 1  $\text{A g}^{-1}$  is showed in

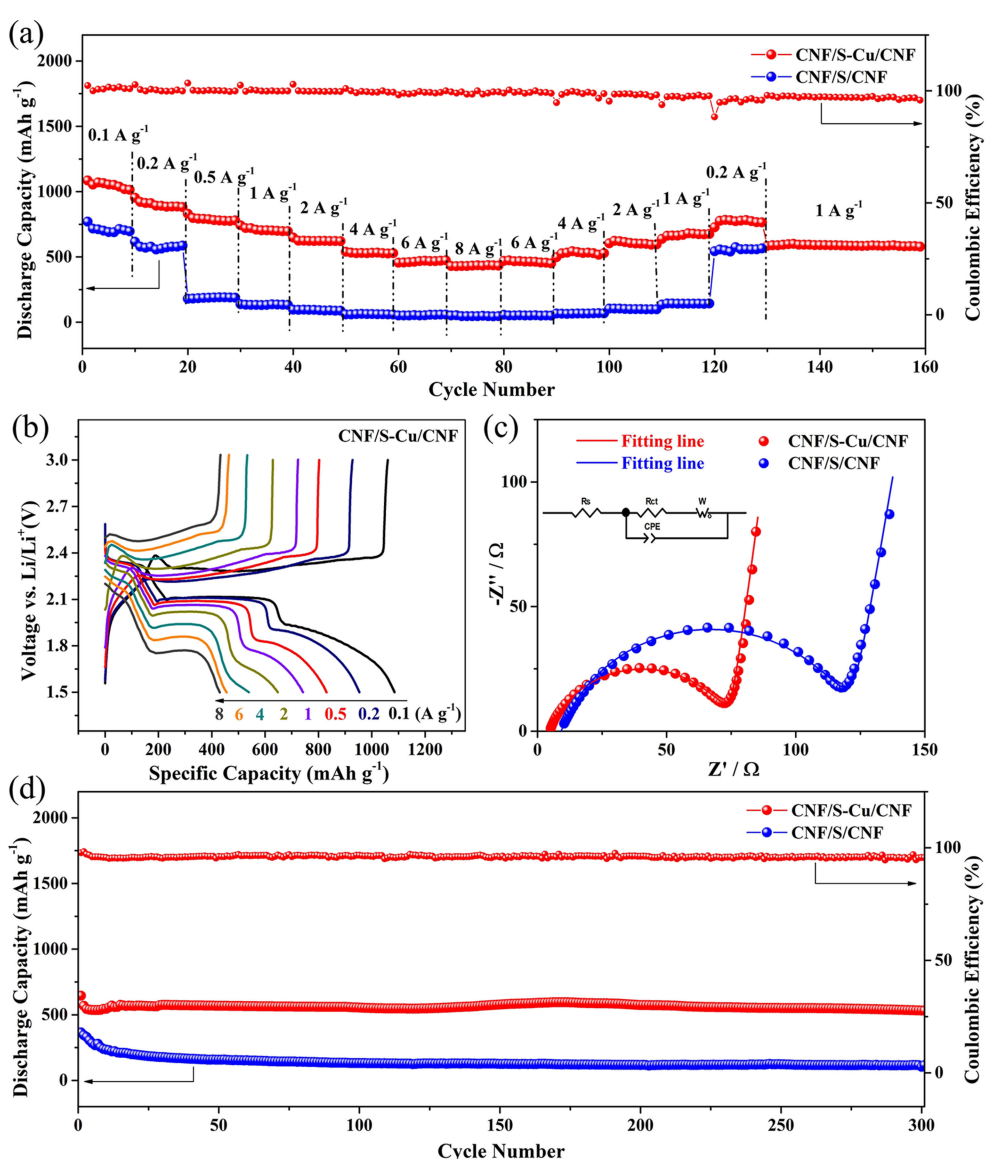


**Figure 5.** a) rate-cycle capabilities of the CNF/S–Cu/CNF and CNF/S/CNF electrodes at various current densities; b) charge/discharge voltage profiles of CNF/S–Cu/CNF electrode at various current densities; c) EIS spectra of CNF/S–Cu/CNF and CNF/S/CNF in Li–S battery before cycling; d) long cycling performance of the CNF/S–Cu/CNF and CNF/S/CNF electrodes at a current density of 1  $\text{A g}^{-1}$ .

Figure 5d. The reversible capacity of CNF/S–Cu/CNF electrode maintains above  $530 \text{ mAh g}^{-1}$  after 300 cycles with the Coulombic efficiency nearly 100%. However, the CNF/S/CNF electrode delivers  $370 \text{ mAh g}^{-1}$  for the first cycle and decrease to  $116 \text{ mAh g}^{-1}$  after 300 cycles. This may be due to the lack of Cu in the CNF/S/CNF electrodes. Without the chemical sulfur fixation by Cu nanoparticles, the cycling capacities of CNF/S/CNF electrode decrease by partial dissolution of polysulfides into the electrolyte. A comparison of Li–S battery using the functional fibers and other carbon matrix is listed in Table S2. Apparently, the cell using functional fiber or self-standing carbon is more attractive in terms of high S utilization under same current density, which is favor for practical Li–S batteries.<sup>[13,29,40,50–58]</sup>

To further confirm the effective physical and chemical sulfur fixation of the sandwich structural CNF/S–Cu/CNF composite during the electrochemical cycling, the cycled batteries are dismantled. The digital photos, SEM cross-section image and the corresponding elements EDS mapping of the CNF/S–Cu/CNF electrodes after 300 charge-discharge cycles are presented in Figure S5. After prolonged electrochemical cycles, the CNF/S–Cu/CNF electrodes still remain good flexible porosity (Figure S5a), which further proved the robust structure of the CNF/S–Cu/CNF nonwoven as cathode for Li–S batteries. As shown in Figure S5b, the CNF/S–Cu/CNF electrodes still maintain the initial sandwich structure with a little wider sulfur interlayer after 300 cycles. This implies the sulfur can be stabilized in this novel structure, achieving endurable electrochemical performance. The main text of the article should appear here with headings as appropriate.

### 3. Conclusions

In summary, we propose and demonstrate a promising flexible sandwich structural nonwoven CNF/S–Cu/CNF composite by electrospinning technology to achieve many simultaneous benefits including high S-loading, robust conductive CNF frameworks and scarcely shuttle effect of polysulfide. As a free-standing cathode for Li–S battery, the CNF/S–Cu/CNF electrode shows excellent rate and cycle performance, exhibiting high reversible specific capacity of  $1295 \text{ mAh g}^{-1}$  at the current density of  $0.1 \text{ A g}^{-1}$  and considerable rate cycling stabilities with capacities retention of around 85% after 300 cycles at a higher current rate of  $1 \text{ A g}^{-1}$ . This novel configuration of the free-standing CNF/S–Cu/CNF electrode exhibits great potential to be a good candidate for commercial flexible and endurable Li–S batteries.

## Experimental Section

### Preparation of CNF–CNF/Cu Double-Layer Films

The CNF–CNF/Cu double-layer films are prepared using high-voltage electrospinning technology and subsequent heat treatment process. Firstly, 0.2 g polyacrylonitrile (PAN, MW = 150000, Aldrich) is dissolved in 2 ml N, N-dimethylformamide (DMF,

Sinopharm Chemical Reagent Co., Ltd.), then put the solution into a micropipettor to prepare for electrospun PAN nanofiber layer. A high voltage of 15 kV is applied for electrospinning PAN nanofibers. The receiving distance between the syringe needle and the receiver is 15 cm, and the injection speed of the syringe pump is  $1.50 \text{ mL h}^{-1}$ . Using the PAN nanofiber film as receiver, another  $\text{Cu}(\text{NO}_3)_2/\text{PAN}$  nanofiber layer is electrospun on the PAN film directly by the same way. Briefly, 0.02 g  $\text{Cu}(\text{NO}_3)_2 \cdot 5\text{H}_2\text{O}$  and 0.2 g PAN are dissolved in DMF to make the electrospinning solution. A high voltage of 10 kV is applied for electrospinning  $\text{Cu}(\text{NO}_3)_2/\text{PAN}$  nanofibers, and the injection speed is  $0.50 \text{ mL h}^{-1}$ . The as-prepared PAN– $\text{Cu}(\text{NO}_3)_2/\text{PAN}$  double-layer films are heated at  $280^\circ\text{C}$  for 2 h in the air atmosphere with  $2^\circ\text{C min}^{-1}$  heating rate for pre-oxidation, hereafter, calcinated to  $800^\circ\text{C}$  for 5 h under a nitrogen atmosphere with heating rate of  $5^\circ\text{C min}^{-1}$  for carbonization. Finally, the CNF–CNF/Cu double-layer films are obtained.

### Preparation of Sandwich Structural CNF/S–Cu/CNF Films

The “Sandwich”-like CNF/S–Cu/CNF electrode is constructed as follows. Firstly, an asymmetrical CNF–Cu/CNF nanofiber is prepared with one part of CNF on another Cu/CNF layer using in-situ electrospinning. Then, an  $\text{S}/\text{CS}_2$  solution (20 wt%) is dropped on the side of Cu-containing nanofibers. Next, another piece of the CNF–Cu/CNF nanofiber loaded S is covered on the as-obtained CNF/S–Cu fibers with the side of Cu-containing fiber contacting sulfur. After dried naturally and heated at  $150^\circ\text{C}$  for 15 min, sulfur impregnate CNF–CNF/Cu films distribute evenly in the free-standing CNF/S–Cu/CNF electrode. For comparison, the sandwich structural CNF/S/CNF films without copper nanoparticles are also prepared in the same way.

### Physical Characterizations

The morphology and elements distribution of the CNF/S–Cu/CNF film are characterized by an FEI Nova SEM 230 equipped with an ultra-high-resolution field-emission scanning electron microscope (FE-SEM) and an energy dispersive X-ray spectrometry (EDS) (INCA X-Max 80, Oxford Instruments). The microstructure of copper nanoparticles in the CNF/S–Cu/CNF film is characterized by a transmission electron microscope (TEM) (JEM-2100F, JEOL, Ltd., Japan). To get the real sulfur contents in the CNF/S–Cu/CNF and CNF/S/CNF films, thermogravimetry (TGA) is recorded with a heating rate of  $5^\circ\text{C min}^{-1}$  in high-purity nitrogen atmosphere by Pyris 1 TGA (PerkinElmer). The X-ray diffraction (XRD) patterns are recorded on a Bruker diffractometer (D8 advance) at 40 kV and 20 mA, with a  $\text{Cu K}\alpha$  radiation in the 2-Theta range from 10 to  $80^\circ$ . The Raman spectroscopies are obtained in a Dispersive Raman Microscope (Senterra R200-L, Germany). The X-ray photoelectron spectroscopy (XPS) data are acquired at room temperature with a Kratos Analytical spectrometer and monochromatic Al  $\text{K}\alpha$  (1486.6 eV) X-ray source.

### Electrochemical Measurements

The Li–S battery measurements are carried out using 2032 two-electrode coin cells at room temperature. The CNF/S–Cu/CNF (and CNF/S/CNF) films are cut into circle discs with a diameter of 12 mm, and the mass loading of sulfur in each electrode is about  $1.2 \text{ mg cm}^{-2}$ . The thickness and weight density of the CNF/Cu support are about  $200 \mu\text{m}$  and  $1.4 \text{ mg cm}^{-2}$ , respectively. The films are directly used as the cathode for Li–S batteries without conducting additive and binder. The coin cells are assembled in the glovebox with lithium metal foils as the counter and reference electrodes, the 1 M lithium bis(trifluoromethanesulfonyl)imide

(LITFSI) in a mixture of 1,3-dioxolane/1,2-dimethoxyethane (DOL/DME, 1:1 v/v) with 0.1 M lithium nitrate ( $\text{LiNO}_3$ ) as electrolyte and microporous polypropylene Celgard 3501 (Celgard, LLC Corp., USA) as the separator, and the volume of electrolyte injected into each coin cell is controlled at  $\sim 60 \mu\text{L}$ .

The galvanostatic charge and discharge performance is tested at various current densities in the potential range of 1.5–3.0 V vs Li/Li<sup>+</sup> by a LAND CT2001A model battery test system (Wuhan Jinnuo Electronics, Ltd.) The specific capacity is calculated corresponding to the mass of active material sulfur. The cyclic voltammetry (CV) tests are implemented using a Gamry instruments (Gamry Co., USA) at a scan rate of  $0.2 \text{ mVs}^{-1}$  within a voltage range of 1.5–3.0 V. Electrochemical impedance spectrum (EIS) measurement is recorded on the same Gamry instruments in the frequency range from 100 kHz to 0.01 Hz.

## Acknowledgements

We gratefully acknowledge the support of the National Science Foundation of China (51671135, 51472161, 21875141). We also acknowledge the support of the Program of Shanghai Subject Chief Scientist (17XD1403000), Shanghai Outstanding Academic Leaders Plan, Shanghai Pujiang Program (18PJ1409000) and the Major Program for the Scientific Research Innovation Plan of Shanghai Education Commission (2019-01-07-00-07-E00015).

## Conflict of Interest

The authors declare no conflict of interest.

**Keywords:** electrochemistry · energy storage · film electrodes · free-standing electrodes · lithium–sulfur batteries

- [1] P. G. Bruce, S. A. Freunberger, L. J. Hardwick, J. M. Tarascon, *Nat. Mater.* **2011**, *11*, 19–29.
- [2] H. J. Peng, J. Q. Huang, X. B. Cheng, Q. Zhang, *Adv. Energy Mater.* **2017**, *7*, 1700260.
- [3] W. Wahyudi, Z. Cao, P. Kumar, M. Li, Y. Wu, M. N. Hedhili, T. D. Anthopoulos, L. Cavallo, L. J. Li, J. Ming, *Adv. Funct. Mater.* **2018**, *28*, 1802244.
- [4] Q. Sun, K. C. Lau, D. Geng, X. Meng, *Batteries & Supercaps* **2018**, *2*, 41–68.
- [5] Z. W. Seh, Y. Sun, Q. Zhang, Y. Cui, *Chem. Soc. Rev.* **2016**, *45*, 5605–5634.
- [6] G. Zheng, Q. Zhang, J. J. Cha, Y. Yang, W. Li, Z. W. She, Y. Cui, *Nano Lett.* **2013**, *13*, 1265–1270.
- [7] H. Pan, X. Huang, R. Zhang, T. Zhang, Y. Chen, T. K. A. Hoang, G. Wen, *J. Solid State Electrochem.* **2018**, *22*, 3557–3568.
- [8] L. Zhou, X. Lin, T. Huang, A. Yu, *Electrochim. Acta* **2014**, *116*, 210–216.
- [9] W. Li, Q. Zhang, G. Zheng, Z. W. Seh, H. Yao, Y. Cui, *Nano Lett.* **2013**, *13*, 5534–5540.
- [10] H. J. Peng, J. Q. Huang, M. Q. Zhao, Q. Zhang, X. B. Cheng, X. Y. Liu, W. Z. Qian, F. Wei, *Adv. Funct. Mater.* **2014**, *24*, 2772–2781.
- [11] H. Chen, C. Wang, Y. Dai, S. Qiu, J. Yang, W. Lu, L. Chen, *Nano Lett.* **2015**, *15*, 5443–5448.
- [12] W. Kang, N. Deng, J. Ju, Q. Li, D. Wu, X. Ma, L. Li, M. Naebe, B. Cheng, *Nanoscale* **2016**, *8*, 16541–16588.
- [13] S. Zheng, F. Yi, Z. Li, Y. Zhu, Y. Xu, C. Luo, J. Yang, C. Wang, *Adv. Funct. Mater.* **2014**, *24*, 4156–4163.
- [14] Y. Pang, Y. Xu, Y. Li, F. Xu, L. Sun, J. Yang, H.-W. Li, S. Zheng, *ACS Applied Energy Materials* **2019**, *2*, 1537.
- [15] Z. Yuan, H. J. Peng, T. Z. Hou, J. Q. Huang, C. M. Chen, D. W. Wang, X. B. Cheng, F. Wei, Q. Zhang, *Nano Lett.* **2016**, *16*, 519–527.
- [16] T. G. Jeong, D. S. Choi, H. Song, J. Choi, S. A. Park, S. H. Oh, H. Kim, Y. Jung, Y. T. Kim, *ACS Energy Lett.* **2017**, *2*, 327–333.
- [17] Y. Du, Z. Yin, J. Zhu, X. Huang, X. J. Wu, Z. Zeng, Q. Yan, H. Zhang, *Nat. Commun.* **2012**, *3*, 1177.
- [18] B. Eckert, R. Okazaki, R. Steudel, N. Takeda, N. Tokitoh, M. Wong, *Top. Curr. Chem.* **2003**, *231*, 32–98.
- [19] T. Z. Hou, X. Chen, H. J. Peng, J. Q. Huang, B. Q. Li, Q. Zhang, B. Li, *Small* **2016**, *12*, 3283–3291.
- [20] J. Song, T. Xu, M. L. Gordin, P. Zhu, D. Lv, Y. B. Jiang, Y. Chen, Y. Duan, D. Wang, *Adv. Funct. Mater.* **2014**, *24*, 1243–1250.
- [21] G. Zhou, F. Li, H. M. Cheng, *Energy Environ. Sci.* **2014**, *7*, 1307–1338.
- [22] D. H. Lim, M. Agostini, F. Nitze, J. Manuel, J. H. Ahn, A. Matic, *Sci. Rep.* **2017**, *7*, 6327.
- [23] S. Tu, X. Chen, X. Zhao, M. Cheng, P. Xiong, Y. He, Q. Zhang, Y. Xu, *Adv. Mater.* **2018**, *30*, 1804581.
- [24] P. Han, T. Yuan, L. Yao, Z. Han, J. Yang, S. Zheng, *Nanoscale Res. Lett.* **2016**, *11*, 172.
- [25] L. Zeng, Y. Jiang, J. Xu, M. Wang, W. Li, Y. Yu, *Nanoscale* **2015**, *7*, 10940–10949.
- [26] W. Weng, V. G. Pol, K. Amine, *Adv. Mater.* **2013**, *25*, 1608–1615.
- [27] M. Agostini, D. H. Lim, S. Bruttii, N. Lindahl, J. H. Ahn, B. Scrosati, A. Matic, *ACS Appl. Mater. Interfaces* **2018**, *10*, 34140.
- [28] H. Yu, H. Li, S. Yuan, Y. Yang, J. Zheng, J. Hu, D. Yang, Y. Wang, A. Dong, *Nano Res.* **2017**, *10*, 2495–2507.
- [29] X. J. Dai, Y. Chen, Z. Chen, P. R. Lamb, L. H. Li, J. du Plessis, D. G. McCulloch, X. Wang, *Nanotechnology* **2011**, *22*, 245301.
- [30] H. Li, Y. Wang, J. Huang, Y. Zhang, J. Zhao, *Electrochim. Acta* **2017**, *225*, 443–451.
- [31] J. H. Yun, J. H. Kim, D. K. Kim, H. W. Lee, *Nano Lett.* **2018**, *18*, 475–481.
- [32] Y. Guo, J. Li, R. Pitcheri, J. Zhu, P. Wen, Y. Qiu, *Chem. Eng. J.* **2019**, *355*, 390–398.
- [33] X. Liang, C. Hart, Q. Pang, A. Garsuch, T. Weiss, L. F. Nazar, *Nat. Commun.* **2015**, *6*, 5682.
- [34] G. Zhou, H. Tian, Y. Jin, X. Tao, B. Liu, R. Zhang, Z. W. Seh, D. Zhuo, Y. Liu, J. Sun, J. Zhao, C. Zu, D. S. Wu, Q. Zhang, Y. Cui, *Proc. Natl. Acad. Sci. USA* **2017**, *114*, 840–845.
- [35] Y. Ge, Z. Chen, S. Ye, Z. Zhu, Y. Tu, X. Yang, *J. Mater. Chem. A* **2018**, *6*, 14885–14893.
- [36] X. Zhao, P. Xiong, J. Meng, Y. Liang, J. Wang, Y. Xu, *J. Mater. Chem. A* **2017**, *5*, 19237.
- [37] L. C. Yin, J. Liang, G. M. Zhou, F. Li, R. Saito, H. M. Cheng, *Nano Energy* **2016**, *25*, 203–210.
- [38] G. Zhou, D. W. Wang, F. Li, P. X. Hou, L. Yin, C. Liu, G. Q. Lu, I. R. Gentle, H. M. Cheng, *Energy Environ. Sci.* **2012**, *5*, 8901–8906.
- [39] H. Zhang, W. Zhao, M. Zou, Y. Wang, Y. Chen, L. Xu, H. Wu, A. Cao, *Adv. Energy Mater.* **2018**, *8*, 1800013.
- [40] G. Li, X. Wang, M. H. Seo, M. Li, L. Ma, Y. Yuan, T. Wu, A. Yu, S. Wang, J. Lu, Z. Chen, *Nat. Commun.* **2018**, *9*, 705.
- [41] Z. Li, Y. Jiang, L. X. Yuan, Z. Q. Yi, C. Wu, Y. Liu, P. Strasser, Y. H. Huang, *ACS Nano* **2014**, *8*, 9295–9303.
- [42] M. Cuisinier, P. E. Cabelguen, S. Evers, G. He, M. Kolbeck, A. Garsuch, T. Bolin, M. Balasubramanian, L. F. Nazar, *J. Phys. Chem. Lett.* **2013**, *4*, 3227–3232.
- [43] Y. Jiang, F. Chen, Y. Gao, Y. Wang, S. Wang, Q. Gao, Z. Jiao, B. Zhao, Z. Chen, *J. Power Sources* **2017**, *342*, 929–938.
- [44] X. Gu, Y. Wang, C. Lai, J. Qiu, S. Li, Y. Hou, W. Martens, N. Mahmood, S. Zhang, *Nano Res.* **2014**, *8*, 129–139.
- [45] D. Ghosh, M. Gad, I. Lau, M. A. Pope, *Adv. Energy Mater.* **2018**, *8*, 1801979.
- [46] Y. Tao, Y. Wei, Y. Liu, J. Wang, W. Qiao, L. Ling, D. Long, *Energy Environ. Sci.* **2016**, *9*, 3230–3239.
- [47] W. Chen, T. Lei, W. Lv, Y. Hu, Y. Yan, Y. Jiao, W. He, Z. Li, C. Yan, J. Xiong, *Adv. Mater.* **2018**, *30*, 1804084.
- [48] D. Xie, X. H. Xia, Y. Zhong, Y. D. Wang, D. H. Wang, X. L. Wang, J. P. Tu, *Adv. Energy Mater.* **2017**, *7*, 1601804.
- [49] R. Fang, S. Zhao, P. Hou, M. Cheng, S. Wang, H. Cheng, C. Liu, F. Li, *Adv. Mater.* **2016**, *28*, 3374–3382.
- [50] M. Agostini, J. Y. Hwang, H. M. Kim, P. Bruni, S. Bruttii, F. Croce, A. Matic, Y. K. Sun, *Adv. Energy Mater.* **2018**, *8*, 1801560.
- [51] Z. Ma, X. Huang, Q. Jiang, J. Huo, S. Wang, *Electrochim. Acta* **2015**, *182*, 884–890.
- [52] Q. Pang, L. F. Nazar, *ACS Nano* **2016**, *10*, 4111–4118.

- [53] F. Nitze, M. Agostini, F. Lundin, A. E. C. Palmqvist, A. Matic, *Sci. Rep.* **2016**, *6*, 39615.
- [54] C. Cavallo, M. Agostini, J. P. Genders, M. E. Abdelhamid, A. Matic, *J. Power Sources* **2019**, *416*, 111.
- [55] L. Xiao, Y. Cao, J. Xiao, B. Schwenzer, M. H. Engelhard, L. V. Saraf, Z. Nie, G. J. Exarhos, J. Liu, *Adv. Mater.* **2012**, *24*, 1176–1181.
- [56] Y. Gong, C. Fu, A. Dong, H. Zhou, H. Li, Y. Kuang, *Batteries & Supercaps* **2018**, *1*, 192; *Supercaps* **2018**, *1*, 192.
- [57] X. Y. Tao, J. G. Wang, Z. G. Ying, Q. X. Cai, G. Y. Zheng, Y. P. Gan, H. Huang, Y. Xia, C. Liang, W. K. Zhang, Y. Cui, *Nano Lett.* **2014**, *14*, 5288.
- [58] C. Zhang, W. Wang, A. Wang, K. Yuan, Y. Yang, Y. Lu, *J. Electrochem. Soc.* **2015**, *162*, A1067–A1071.

---

Manuscript received: January 31, 2019

Revised manuscript received: March 4, 2019

Accepted article published: March 6, 2019

Version of record online: March 19, 2019

---